Supplemental Data

Animal Models

Orthotopic transplantation of KPr and KPAr into lungs of syngeneic C57BL/6J mice was performed as previously described (Breitenecker K et al 2021). Briefly, tdTomato$^+$ (tdTom$^+$) KP cells (KPr) were isolated from K-ras^{G12D} mutant and p53 deficient, autochthonous mouse lung tumors. A20 was knocked out in these cells using CRISPR/Cas9 technology to generate KPAr cells. For orthotopic transplantation, 1×10^6 KPr or KPAr cells were suspended in serum- and antibiotic-free RPMI 1640, supplemented with 0.01M EDTA, and instilled intra-tracheally into anesthetized (Ketamine-Xylazine mixture) male and female 7-9 weeks old C57BL/6J mice (Moll HP et al. 2021); naïve age-matched C57BL/6J mice were used as the wild-type (WT) cohort. In total, n=72 mice (WT: n=32, KPr: n=24, KPAr: n=28) were used for PET imaging and ex vivo autoradiography (n=17), radioFlow (n=29 plus n=2 for assessment of Cherenkov radiation), conventional fluorescence-activated cell sorting (n=12) and in vitro immune cell culture (n=12).

In vivo Imaging and quantification

Throughout the imaging procedure, animals were maintained under anesthesia and kept warm on a 37°C positioning bed. The depth of anesthesia was adjusted based on the monitored respiratory rate.

The CT raw data were reconstructed with a Feldkamp algorithm followed by standard mouse beam-hardening correction and noise reduction (matrix size: 1024×1024; effective pixel size: 97.56 µm). The dedicated CT image data were calibrated to Hounsfield Units (HU). PET list mode data were sorted into three-dimensional sinograms and reconstructed using OSEM 3D/filtered back projection (FBP) without scatter correction and ramp filter (matrix size 256×256). The data were normalized and corrected for random, dead time, attenuation, and radioactive decay. A calibration factor was applied to convert the activity information into absolute concentration units.

Multimodal (µPET/CT) rigid-body image co-registration and biomedical image quantification was performed using the image analysis software PMOD 3.8 (PMOD Technologies, Fällanden, Switzerland). Volumes of interest (VOIs) for total lung as well as for individual lung tumor lesions were created based on the CT images before fusing them to the respective PET images. For tumor lesions, VOIs were annotated in several lesions and normalized to the lesion number based on PET to extract the metabolic tumor volume

(MTV [mL]). The tracer uptake in the VOIs was normalized to the injected dose and animal weight and expressed as mean standardized uptake value (SUV_{mean} [g/mL]). Additionally, the tumor-to-liver ratio and the total lesion glycolysis (TLG) was calculated by multiplying the tumor SUV_{mean} with the corresponding MTV to facilitate the comparison between animals. Following the μPET/CT scan, still anesthetized mice were sacrificed by cervical dislocation. Lungs were harvested, weighted and the organ-specific radioactivity was measured in a gamma counter (Hidex AMG, Turku, Finland). After decay correction, results were expressed as percent of the injected dose of radioactivity per gram of tissue [%ID/g]. Following gamma counting, the lungs were processed for either radioFlow analyses or ex vivo autoradiography and histology.

Fluorescent monoclonal antibody (mAb) staining (cocktails):

Cocktail 1: (eFluor450)-CD45 (1:400, #48-0451-82, eBiosciences), (BV605)-CD11b (1:800, #101237, BioLegend), (PE-Cy7)-F4/80 (1:400, #123114, BioLegend), (AF488)-CD86 (1:200, #105018, BioLegend) and (AF700)-CD206 (1:200, #141734, BioLegend); see gating strategy in **Supplemental Fig. 3A**.

Cocktail 2: (APC-Cy7)-CD3 (1:200, #100222, BioLegend), (eFluor450)-CD45 (1:400, #48-0451-82, eBiosciences), (BV605)-CD11b (1:800, #101237, BioLegend), (FITC)-CD4 (1:400, #11-0041-82, eBiosciences), (APC)-CD8 (1:400, #17-0081-82, eBiosciences) and (PE-Cy7)-F4/80 (1:400, #123114, BioLegend); **Supplemental Fig. 3B**.

Cocktail 3: (APC-Cy7)-CD3 (1:200, #100222, BioLegend), (eFluor450)-CD45 (1:400, #48-0451-82, eBiosciences), (PE)-CD19 (1:400, #557399, BD Biosciences), (BV605)-CD11b (1:800, #101237, BioLegend) and (PE-Cy7)-F4/80 (1:400, #123114, BioLegend); **Supplemental Fig. 3C**.

Ex vivo autoradiography and immunofluorescence staining of lung tissue

Radioactive lung tissue samples were snap-frozen in liquid N_2 and sectioned using a micro-cryotome (CryoStar NX70, Epredia, Kalamanzoo, MI, USA). Serial frozen sections were thaw-mounted onto superfrost slides (Menzel-Gläser SUPERFROST® PLUS, Thermo Scientific, Braunschweig, Germany): 20 μm slides were put on Phosphor Imager plates (Multisensitive Phosphor Screens Long Type MS, PPN 7001724, PerkinElmer) for autoradiography (AURA); 10-20 μm proximate slides were processed for immunofluorescence (IF) staining. Autoradiographic images were analyzed with a Phosphor Imager (CR-35 Bio, Elysia-raytest GmbH, Straubenhardt, Germany) and data analysis was performed with a dedicated

software (AIDA Image Analysis Software) using the intensity [QL], corrected for background intensities [QL-BKG]. QL-BKG was converted to Bq based on a fluorine-18 calibration curve. After half-life corrections and correcting for the applied dose, the %ID was calculated for each AURA slide.

Immunofluorescence (IF) staining was performed on the frozen sections previously cut and stored at -80°C. To conserve the cell innate tdTomato in the tissues, all steps were done with minimal exposure to ambient light. First the slides were taken from -80°C and left to thaw for 10 min, followed by three washes in TBS (50 mM tris base (#T1503-5kg, Sigma-Aldrich, USA), 154 mM NaCl (#S9625-5kg, Sigma-Aldrich, USA) in H_20). Slides were then fixed using -20°C cold acetone (#5025.2, Carl Roth, Germany) at -20°C for 10 min and then washed three times with TBS at room temperature. A solution of 5% normal goat serum (#S-1000, Vector Laboratories, USA) + 1% bovine serum albumin (BSA, #A7906-500G, Sigma-Aldrich, USA) in TBS was applied for 1 h at room temperature to block unspecific binding from the secondary antibody. Slides where then washed two times with TBS and one time with TBST, (TBS + 0,1% Tween-20 (#P9416, Sigma Aldrich, USA)) the following washing steps after incubations followed the same regimen. F4/80 antibody (1:400, #30325, #70076S, Cell Signaling Technology Europe B.V., Netherlands) was diluted in TBS containing 1% BSA and incubated overnight at 4°C. After primary antibody incubation the slides were washed, goat anti rabbit AF600 antibody used as secondary antibody (1:2000, #A-21074, Life Technologies, USA) was diluted in TBS with 1% BSA, incubated for 1 h at room temperature and subsequently washed. To stain the nuclei a DAPI solution (0.2 µg/ml, #B422801, Biolegend, USA) was applied for 10 min. This was followed by three washing steps with TBS. Slides where then mounted with Fluoromount-G (#00 4958 02, Invitrogen, USA) and kept at 4°C until imaging. Image acquisition was performed using a TissueGnostics scanning microscope utilizing TissueFAXS software suite (TissueFAXS 7.0 Built 6245.0137, TissueGnostics GmbH, Austria).

Immune cell isolation and in vitro cell [^{18}F]FDG uptake analysis

Immune cells were isolated from WT mice. Dulbeccos's modified Eagle's medium (DMEM) was purchased from Thermo Fischer Scientific (Waltham, MA, USA) and supplemented with 10% fetal calf serum (FCS) and 100 U/mL penicillin and 100 µg/mL streptomycin. All cells were maintained at 37°C with 5% CO_2 in a humidified incubator.

For macrophage isolation (**Supplemental Fig. 4A**), femur and tibia were flushed with PBS containing 1% FCS to collect the bone marrow, subsequent erythrocytes were removed. To differentiate bone marrow-derived cells into macrophages, 20 ng/mL M-CSF (BioLegend, San Diego, CA, USA) was added to the culture medium (DMEM). After 6 days of culture in 6-well plates, macrophages were activated into MΦ1 macrophages by the addition of fresh cell culture medium containing 100 ng/mL of lipopolysaccharide (LPS) (Sigma Aldrich) and 20 ng/mL interferon-γ (IFN-γ) (Merck). For activation into MΦ2 macrophages, 10 ng/mL IL-4 were added. The medium was also changed for untreated macrophages (MΦ0), but no LPS, IFN-γ, or IL-4 was added. On day 7, macrophages were washed with cold PBS, scraped from the flask and used for further in vitro experiments.

CD4 and CD8 T cells were isolated (**Supplemental Fig. 4B**) by a MACS column system (Miltenyi, Bergisch Gladbach, Germany) and resuspended in DMEM containing 1% 1M HEPES buffer (PAN-Biotech GmbH, Aidenbach, Germany), 1% 100 mM sodium pyruvate solution, 1% MEM amino acids and 500 µM β-mercaptoethanol (all from Sigma Aldrich). Cells were cultured in 6-well plates prepared 24 h in advance with either phosphate-buffered saline (PBS) supplemented with 0.5 µg/mL anti-CD3 and 5 µg/mL anti-CD28 antibodies (both purchased from BioXcell, Lebanon, NH, USA) or exclusively with PBS (naïve condition/non-activated T cells). On the subsequent day, 50 U/mL IL-2 (Novartis, Basel, CH) and 0.5 ng/mL IL-7 (Thermo Scientific, Waltham, MA, USA) were added to the cells cultured with anti-CD3/anti-CD28 (activated T cells: $CD4^+/CD8^+$). After another 24 h, the cells (non-adherent) were harvested and used for in vitro experiments.

Macrophages (MΦ0, MΦ1 and MΦ2) and T cells (activated and non-activated CD4/CD8) were diluted with PBS to 10^5 cells/90 µL and incubated in 96-well filter plates (MADVN6550) with 60 µL of 0.4 MBq/mL [^{18}F]FDG. After 60 min incubation at 37°C, the cells were washed as described above, transferred into tubes using a commercial punch kit (MAMP09608) and measured in a gamma counter (Wizard 2, PerkinElmer). Uptake was quantified as the percentage of added radioactivity.

Fluorescence-activated cell sorting of lung tissue and in vitro [^{18}F]FDG cell uptake analysis

Lung tissue samples from WT, KPr and KPAr mice (without being injected with [^{18}F]FDG) were used for conventional fluorescence-activated cell sorting. To obtain T cells, B cells, macrophages and tumor cells,

cell suspensions were sorted with mAb-cocktail 3 (see details above). For in vitro cell uptake, all experiments were performed using a filtration system (Merck MultiScreen™HTS Vacuum Manifold, Merck Millipore, Darmstadt, Germany) for high throughput cell uptakes. Therefore, cell numbers standardized to 10^5 cells/90 µL PBS were used for F4/80$^+$, CD3$^+$, CD19$^+$ and tdTom$^+$ tumor cells (the later only for KPr and KPAr). The respective cell suspensions (90 µL) were incubated in 96-well filter plates (MADVN6550) with 60 µL of a 0.4 MBq/mL radiotracer solution (PBS) in a cell incubator (37°C, 5% CO_2 and saturated humidity). To assess unspecific binding, the filter plates alone were incubated with the same [^{18}F]FDG concentration under identical conditions. After 60 min of incubation, the cells were washed with PBS (2 × 200 µL) by vacuum filtration through the plate. The filters containing the cells were individually transferred into tubes using a commercial punch kit (MAMP09608, Merck) and measured in a gamma counter (Wizard 2, PerkinElmer). Additionally, 60 µL of the 0.4 MBq/mL radiotracer solution were separately measured in the gamma-counter to quantify the maximum amount of added radioactivity/well (100% [^{18}F]FDG). Cell uptake was quantified as percentage of added radioactivity and corrected for unspecific radiotracer binding on the filter plates.

Statistical analysis

Statistical analyses were performed in GraphPad Prism 9 (GraphPad Software, Inc., San Diego, CA, USA). Values are represented as arithmetic means ± standard error (SD). Statistical significance was calculated with nonparametric Student's t-test when comparing two groups or with two-way ANOVA plus Tukey's multiple comparisons test when comparing more than two groups. Significance is indicated in the figures by *: p-value < 0.05; **: p-value < 0.01; ***: p-value < 0.001; ****: p-value < 0.0001.

Supplemental Results and Discussion:

RadioFACS analysis using mAb-cocktail 3

The cell distribution revealed that the highest cell type fraction was CD19$^+$ cells (B cells) with 46% for KPr and KPAr, followed by tumor cells (tdTom$^+$) with 23% each, MΦ (F4/80$^+$) and CD3$^+$ T cells both accounting for 16% in the KPr mice and 21% for MΦ and 9% for CD3$^+$ cells in KPAr mice. Analysis of the [^{18}F]FDG

distribution among the cell fractions showed the highest uptake in the B cell fraction (54%), followed by MΦ with 31%, T cells with 10% and 5% for the tumor cells in KPr mice. For KPAr mice, the percentages were 53%, 35%, 4%, and 8%. Normalization of the [^{18}F]FDG cell uptake to 10^5 cells revealed that MΦ had the highest uptake in both groups, followed by B cells, T cells and the lowest [^{18}F]FDG uptake was observed in tumor cells (51>29>14>6% for KPr and 46>32>14>9% for KPAr). No significantly differences were found between the groups in cell type distribution or glucose metabolism (details see **Supplemental Table 1**, **Supplemental Fig. 2**).

It is important to note that the respective sorting scheme significantly influences the relative distribution of the cells. In this study we have used three panels to depict the whole lung tissue cell composition. This allowed us to also quantify tumor lesions, which are too small for surgical dissection, or even cells from tumor-draining lymph nodes. Furthermore, using the total lung and three different mAb-cocktails minimize the error of missing surrounding stromal immune cells. Moreover, we could quantify the contribution of [^{18}F]FDG B cell uptake within the lung, potentially coming from lymph nodes, as well as structural cells.

In vitro cell uptake of [^{18}F]FDG

To cross-correlate our ex vivo radioFlow results, in vitro [^{18}F]FDG cell uptake experiments were conducted. Therefore, non-radioactive lung tissues of WT (n=4), KPr (n=4) and KPAr (n=4) mice, of which n=2 per group were pooled prior to flow cytometry, were sorted (mAb-cocktail 3) and the radiotracer was subsequently added to the sorted and normalized (10^5) cell fractions. Consistent with the radioFlow findings of this panel (**Supplemental Fig. 2B**), the in vitro assay showed that the highest [^{18}F]FDG uptake was in MΦ ranging from 4-7% [^{18}F]FDG uptake/10^5 cells (WT: 3.98±2.75%, KPr: 6.93±9.51%, KPAr: 3.93 ± 3.74%) and only 0.15-0.7% in tumor cells (KPr: 0.66±0.76%, KPAr: 0.15±0.14%). Healthy WT lungs do not harbor tdTom$^+$ cells, therefore no [^{18}F]FDG uptake is shown (**Supplemental Fig. 5A**). B cells (WT: 0.26%, KPr: 0.51%, KPAr: 0.75%) and T cells (WT: 0.16%, KPr: 0.30%, KPAr: 31%) exhibited similar ranges of uptake (from n=2 pooled lung tissues, and hence only one biological replicate). Overall, we observed the same pattern of [^{18}F]FDG uptake between the in vitro and radioFlow experiments.

The [^{18}F]FDG uptake was further investigated in different MΦ subpopulations. As MΦ1 could not be detected in vivo, bone marrow cells from WT mice were collected, cultured (MΦ0) and further differentiated

into MΦ1 and MΦ2. MΦ0 tended to have the lowest uptake (7.5±3%/10^5 cells), while both MΦ1 and MΦ2 showed similar uptake values of 12±2.8% and 10±5%, respectively (**Supplemental Fig. 5B**, n=6 WT mice). With regard to immunotherapy, we evaluated the impact of T cell subtypes and their activation on the [^{18}F]FDG uptake. Therefore, CD8 and CD4 T positive cells were isolated and activated. The average [^{18}F]FDG uptake ranged from 0.32 to 0.42%/10^5 cells and did not differ between subtypes regardless and activation status (**Supplemental Fig. 5C**, n=6 WT mice). Additionally, T cell uptake was approximately 10 times lower than that of MΦ, suggesting that T cells may depend on other nutritional supply chains rather than solely glucose.

Cherenkov radiation

Initially, we did not observe any differences in sorting efficiency or cell population between radioactive and non-radioactive lung tissue. Nevertheless, and in addition to analyzing the autofluorescence of biological material, we also investigated the effects that might occur due to Cherenkov radiation emitted by fluorine-18 decay.

Cherenkov light measurements were performed using the IVIS® Spectrum (PerkinElmer Inc.) in vivo imaging system setting for Cherenkov and regions of interest were annotated. In detail, [^{18}F]FDG was diluted in 0.9% sodium chloride solution to activity concentration ranging from 0.16 to 2 MBq. 1.5 mL transparent Eppendorf reaction vials were completely filled with the respective solution to avoid air pockets. In addition, each measurement contained a reaction vessel filled with only 0.9% sodium chloride solution to quantify and correct the background. The reaction vials were annotated with same size egg-shaped ROIs covering the vial. For the cross calibration, an aliquot of each prepared [^{18}F]FDG dilution was counted using a Hidex AMG Gamma counter. The exported data from Cherenkov light imaging and gamma counting were exported and correlated with Excel, and the calibration curve equation was used to calculate the Cherenkov light using the same activities used in the radioFlow acquisition.

Representative images of the filled vials and radioactive organs (lung, liver, muscle, fat) as well as the calibration curve (R^2=0.9913) can be seen in **Supplemental Fig. 6**. The lowest dose represents 0.16 MBq, which is the average of the total lung activity corrected to the injection time. This value represents the lower limit of quantification (LOQ) of the IVIS (10-time background signal). Using the calibration curve and the

activity counts measured for the single cell fraction after cell sorting and corrected to the time of the sorting, the Cherenkov signal could be calculated. As the activities measured in the single cell fractions are in the kBq range (not exceeding 207 kBq), a single cell or a few cells within the cell sorting stream cannot produce a measurable signal. Therefore, we conclude that the Cherenkov radiation cannot be measured within the FACS detection and after at least one half-life. We went one step further and used the FACS on radioactive but unstained tissue to see if the cell sorting system is detecting any Cherenkov radiation. As expected, the cell sorting system was not able to detect Cherenkov radiation (**Supplemental Fig. 7**). Therefore, we conclude that the maximum dose of [^{18}F]FDG (30±3 MBq) administered in this study does not affect the sorting results and could even be increased.

Dose rate calculation

Dose rate was calculated for the duration of the sorting time. It is important to note that the cell sorters are mostly and world-wide located in non-radioactive areas and beside a few millimeters of aluminum device cover unshielded. Therefore, we used the maximum activities ever measured of the cell suspension and calculated the dose rate unshielded and 30 cm distance from the source for two organs. The dose rates were calculated using the dose rate calculator, Rad Pro Calculator. The maximum measured activities of the cell suspensions from spleen and tumor tissue/lung tissue were used to calculate the dose rate based on both energy windows of fluorine-18, and a distance of 30 cm (closest distance of the devise operator) and no shielding. The results are expressed as microSv or mSv per hour and the year dosage was calculated for eight experiments.

For spleen tissue the mean value was 90 kBq and for lung and respectively tumor tissue 207 kBq. Hence, resulting in a maximum dose rate per year of 0.005 mSv/a, which is equivalent to a dental x-ray or a yearly intake of 40-50 bananas and do not add significant higher amount to the yearly dose rate for general population of in average 2.4 Sv/a world-wide (**Supplemental Table 2**).

Supplemental Discussion including Limitations:

We need to state that cell distribution depends highly on the selected panel and cell sorting device. To depict the entire distribution of [^{18}F]FDG-uptake across all cellular subtypes, we used a panel sorting all the significant fractions of lung composition, including structural cells like epithelial cells (mAb-cocktail 1). Also, we sorted the whole lung and not the dissected tumor lesion. We could find a high number of B cells in the sorted tumor lung tissue, which might indicate a contribution of lymph nodes to the overall [^{18}F]FDG signal. However, by correlating our findings with immunofluorescence and autoradiography, we could depict the heterogeneity of the tumor tissue and surrounding immune cells. Additionally, isolating only the tumor lesions might have lowered the total counts or might have need injection of higher activity doses. An alternative could be pooling tumor lesions from the same group for cells with lower tracer uptake to reach LOQ, but the heterogeneity of the tumor lesions within the same mouse must also be considered. Nevertheless, in all panels, the uptake of [^{18}F]FDG was the most prominent in immune cells and the lowest in tumor cells.

While other studies report similar methods (Hesketh RL et al. 2019; Bartos LM et al. 2022; Reinfeld et al. 2021; Das N et al. 2024 & Deng S et al. 2023), it is noteworthy that our approach allows for the correction of %ID and expands on the limit of detection (LOD) and limit of quantification (LOQ, defined as three and ten times the background) of the respective gamma counts. In detail, those studies reported low CPM values in the extrapolated data (normalized to a certain cell number) and no background values or correction were indicated. Additionally, only CPM without any normalization or CPM/cell number were depicted: absolute CPM might be affected by different injected doses as well as it does not give a full picture on the recovery (for example missing cell fractions from using negative selection magnetic bead sorting). Total CPM distribution (%CPM of all cell fractions) impacts the interpretation of the PET images, while the normalized CPM for the cell number are not representative of the PET images. Normalization to the cell number is important but solely a direct comparison of the metabolic activity or [^{18}F]FDG uptake/cell. Moreover, some studies used significantly higher radioactivity amounts (up to 145 MBq for fluorine-18), if they were specified at all, and therefore imaging results and ex vivo results might not be comparable due to detection limits of the dedicated µPET system. The required starting activities will depend on the prevalence of cells as well as their metabolic activity or target expression. Hence, it is not possible to state general rules for tracer application and conducting pilot experiments will be necessary to adjust accordingly.

We found structural cells in the lung to be sometimes below LOD and therefore in the range of the background activity. As the number of T cells was very low, also in some cases the LOQ could not be reached (e.g. during technical problems that delayed the measurement of the samples). In general, for cells with low [^{18}F]FDG metabolism, we have found that 150 to 200 thousand cells are required for LOD and LOQ. For the cells with the highest uptake (MΦ), 30 thousand cells were already sufficient to measure signals above LOD or even LOQ. Depending on the pharmacokinetics (distribution phase till equilibrium) and radioactive half-life, we expect half-lives similar to or longer than fluorine-18 to be suitable for radioFlow. Additionally, if the target organ does not require enzymatic digestions for cell suspension preparation, gallium-68 might be an additional candidate for radioFlow, despite its short half-life of 68 min. The duration of our full protocol, starting from radiotracer application to the final radioactive counting of the sorted single cell suspensions, was below 4 hours in contrast to reported times of up to 5.3 hours.

So far, no dose rates for the operator or even biological effects on immune or tumor cells from radioactivity dose rates have been considered. Our study revealed that there is no significant increase of radiation dose rate per year for the users. For instance, conducting 40 measurements with the highest measured activity would result in a dose rate of 0.005 mSv/a, equivalent to that of a single dental x-ray (**Supplemental Table 2**).

Furthermore, we excluded that Cherenkov radiation affects our cell sorting at the radioactivity levels applied in our study (**Supplemental Fig. 6 and 7**). Studies with considerably higher amounts should consider the potential effect of Cherenkov signals on cell sorting. Conversely, we consider Cherenkov radiation as a potential tool to sort cells based on this signal in future studies.

Thus, we present a robust and reliable in vivo method to explore the metabolic interactions in tumor tissue using short-lived radionuclides as fluorine-18. Importantly, this method can be extended to analyze any organ with the advantage that lymphoid organs usually do not require the digestion step, allowing for faster processing.

Lastly, it is important to note that the results only represent a robust and reliable conclusion regarding [^{18}F]FDG uptake and distribution, but not on glucose or [^{18}F]FDG metabolism itself. Exploring changes in [^{18}F]FDG metabolism and identifying pathways beyond [^{18}F]FDG-6-P (Patronas E-M et al. 2023), could be insightful for understanding cancer and TME metabolism as well as metabolite competition. Ultimately, the

broader objective is to unravel the intricate mechanisms of immune cell activation and exhaustion mediated by intermediates and metabolites across various glucose and other metabolic pathways. Hence, other techniques need to be combined with radioFlow as metabolomics using LC-MS or transcriptomics.

However, since most [^{18}F]FDG metabolites are subject to trapping mechanisms or further metabolized in the cytosol and mitochondria, we anticipate that variations in metabolism would likely not alter our findings on overall [^{18}F]FDG uptake. Also, the combination of other methods comes with additional challenges: Automated cell sorting can significantly impact cellular metabolism, presenting a challenge for metabolomic studies. An alternative approach is magnetic-activated cell sorting (MACS), which offers gentler cell isolation. However, when using positive selection, it is critical to ensure that potential effects from the magnetic beads or residual antibodies are excluded to avoid confounding the results.

Supplemental Figures:

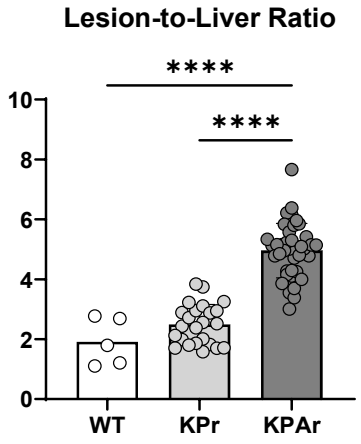

Supplemental Fig. 1: Image based quantification of tumor lesion-to-liver ratio based on [^{18}F]FDG SUV_{mean} of volume of interests (VOIs) in healthy lung tissue (WT: n=5) and lesions (KPr: n=24, KPAr: n=40). ****p<0.0001.

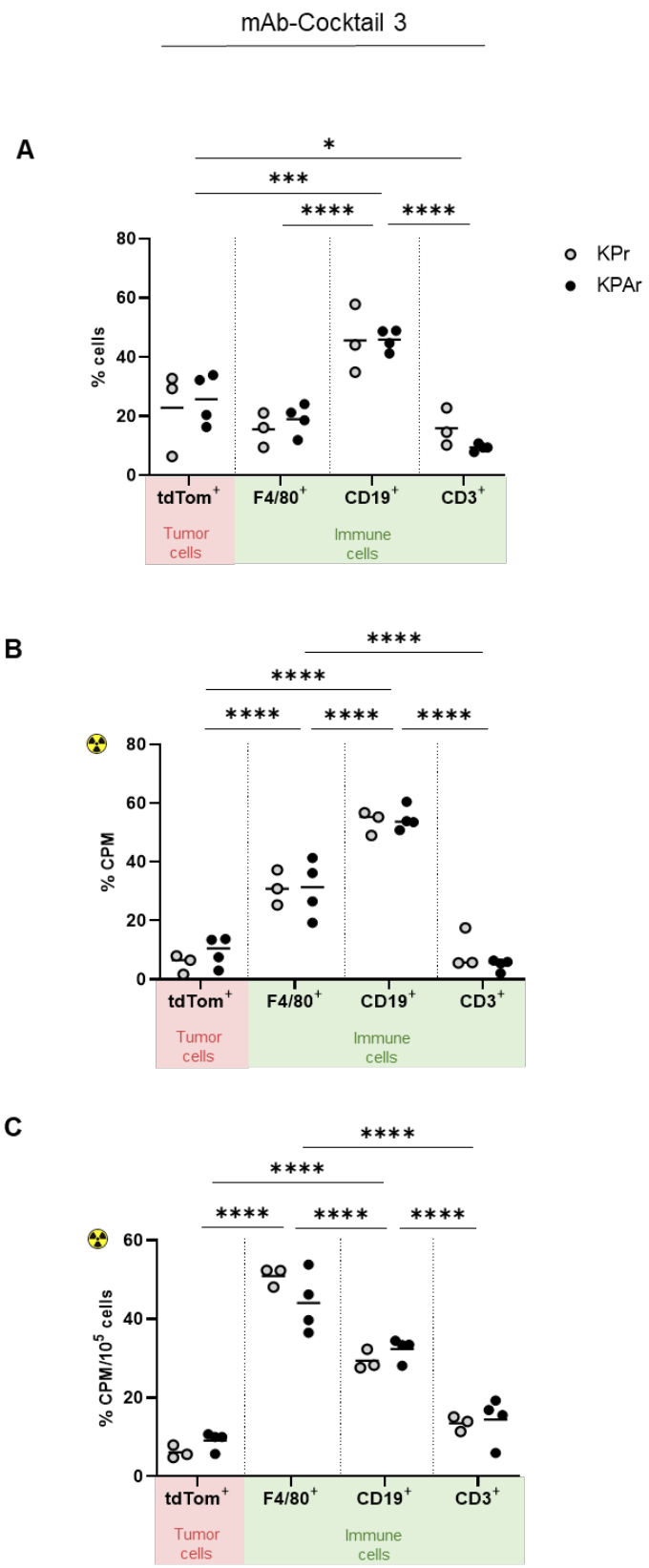

Supplemental Fig. 2: Sorted cell type distribution within the lungs of WT, KPr and KPAr mice (**A**). In vivo [^{18}F]FDG uptake in sorted cells from whole lung of KPr and KPAr mice (**B**). In vivo [^{18}F]FDG uptake normalized to sorted cell number from whole lung of KPr and KPAr mice (**C**), n≥3. CPM = counts per minute (measured in gamma counter).

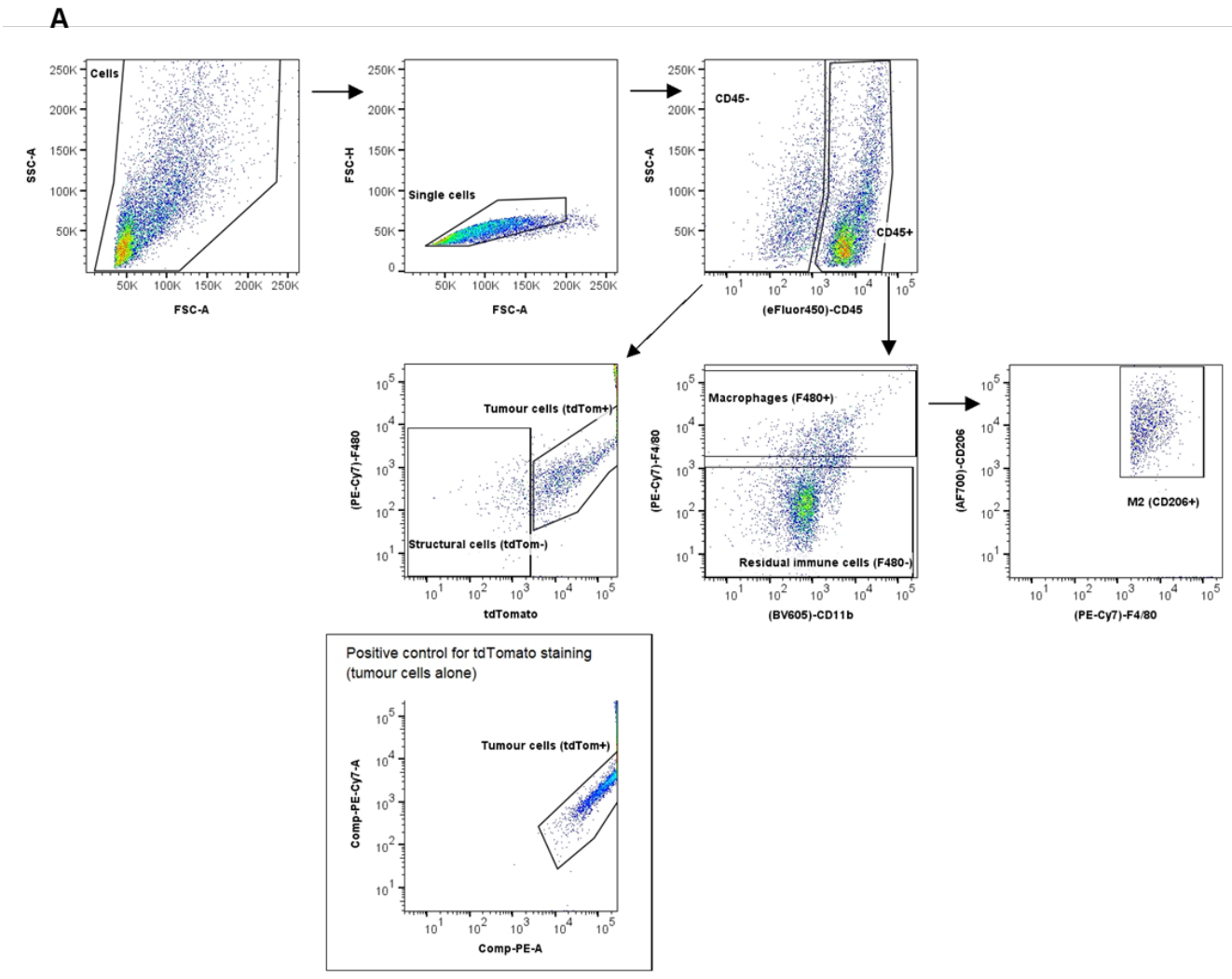
A
Cells
SSC-A
FSC-A
Single cells
FSC-H
CD45-
CD45+
(eFluor450)-CD45
Tumour cells (tdTom+)
Structural cells (tdTom-)
(PE-Cy7)-F480
tdTomato
Macrophages (F480+)
Residual immune cells (F480-)
(PE-Cy7)-F4/80
(BV605)-CD11b
M2 (CD206+)
(AF700)-CD206
Positive control for tdTomato staining
(tumour cells alone)
Comp-PE-Cy7-A
Comp-PE-A
B
Tumor cells (tdTom+)
T cells (CD3+)
(APC-Cy7)-CD3
CD8+
CD4+
(APC)-CD8
(FITC)-CD4

C

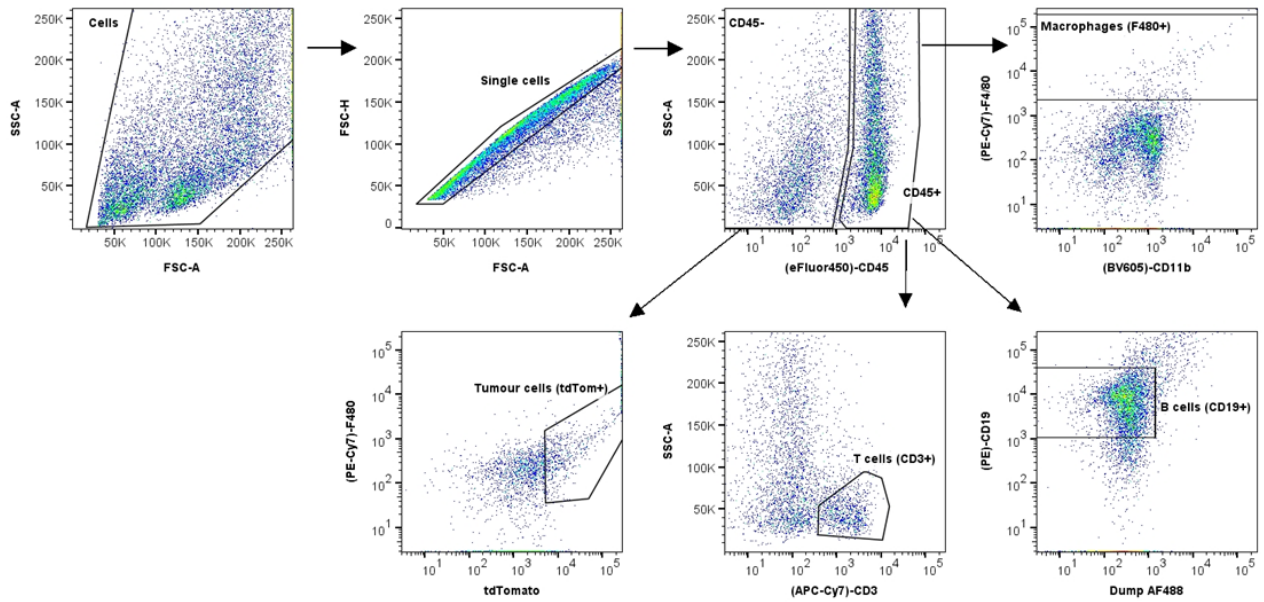

Supplemental Fig. 3: Representative gating strategy for the cell sorting using mAb-cocktail 1 (KPAr) (**A**), mAb-cocktail 2 (KPr) (**B**) and mAb-cocktail 3 (KPAr) (**C**).

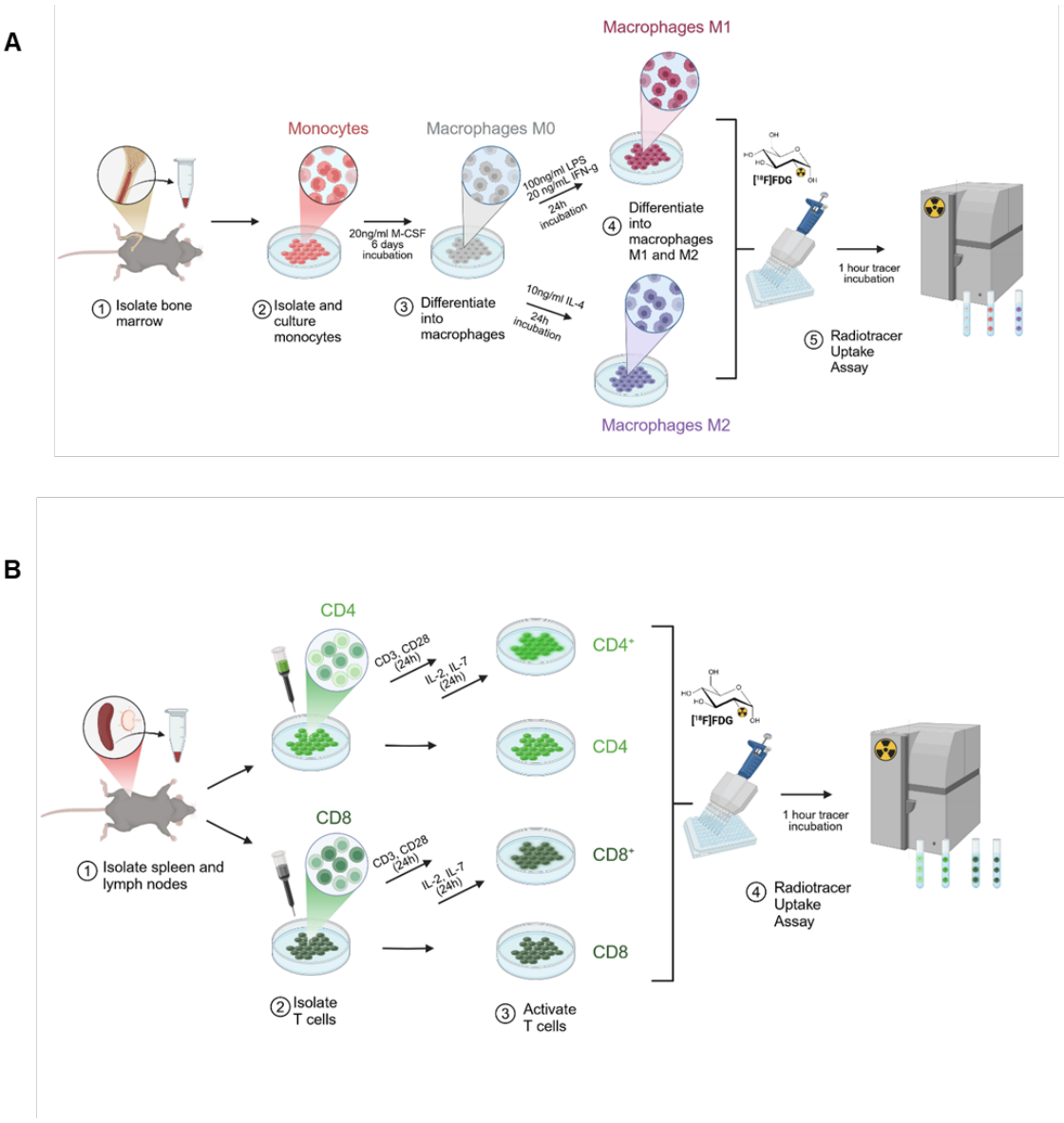

Supplemental Fig. 4: Scheme of macrophage isolation, differentiation and [^{18}F]FDG uptake (**A**). Scheme of T cell isolation using magnetic cell sorting, activation protocol and [^{18}F]FDG uptake measurements (**B**). Created with BioRender.com.

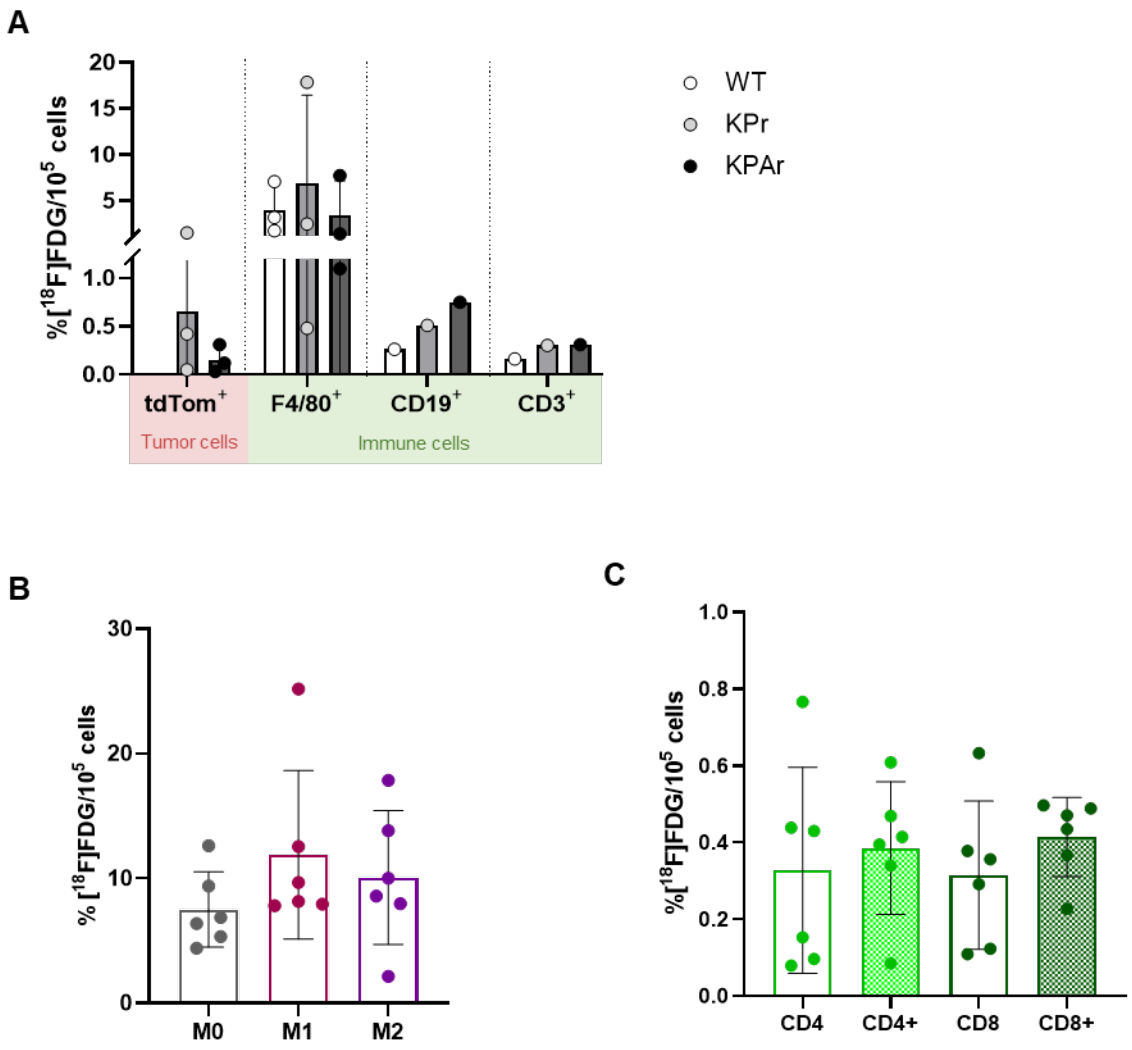

Supplemental Fig. 5: In vitro [^{18}F]FDG uptake in different lung cell types after 60 min of incubation. [^{18}F]FDG uptake in different sorted cell types normalized to the cell number, corrected for unspecific binding and expressed as % of total added radioactivity, n=1-3 (each data point is the mean of three technical replicates) (**A**). Macrophage uptake of [^{18}F]FDG; n=6 (each data point is the mean of at least two technical replicates) (**B**). T cell uptake of [^{18}F]FDG, n=6 (each data point is the mean of at least two technical replicates) (**C**).

A

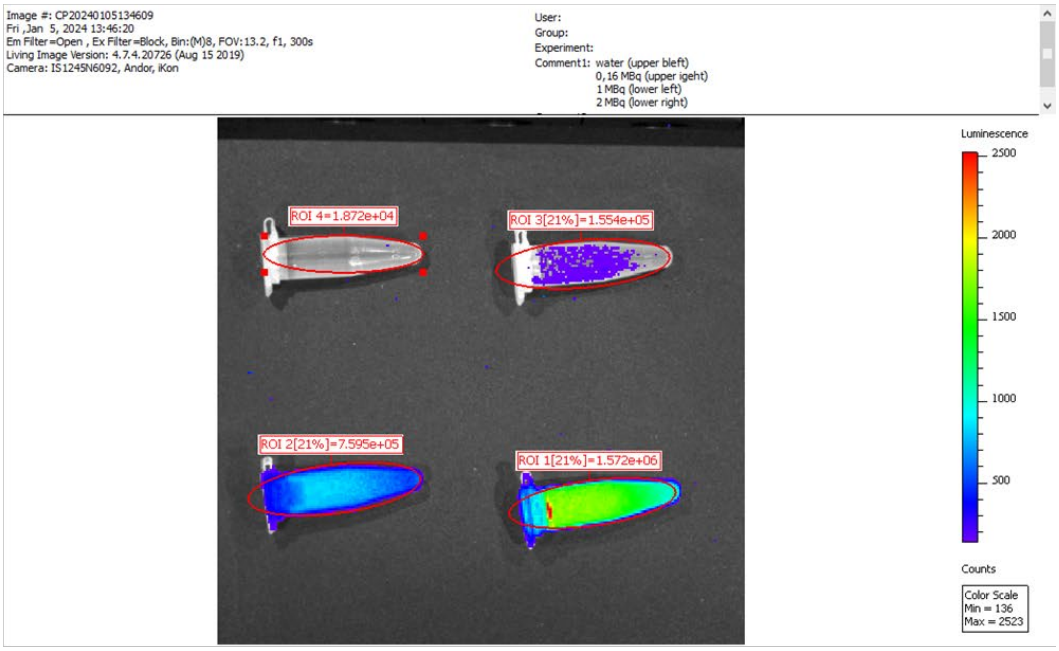
Image #: CP20240105134609
Fri ,Jan 5, 2024 13:46:20
Em Filter=Open , Ex Filter=Block, Bin:(M)8, FOV:13.2, f1, 300s
Living Image Version: 4.7.4.20726 (Aug 15 2019)
Camera: IS1245N6092, Andor, iKon
User:
Group:
Experiment:
Comment1: water (upper bleft)
0,16 MBq (upper igeht)
1 MBq (lower left)
2 MBq (lower right)
ROI 4=1.872e+04
ROI 3[21%]=1.554e+05
ROI 2[21%]=7.595e+05
ROI 1[21%]=1.572e+06
Luminescence
2500
2000
1500
1000
500
Counts
Color Scale
Min = 136
Max = 2523

B

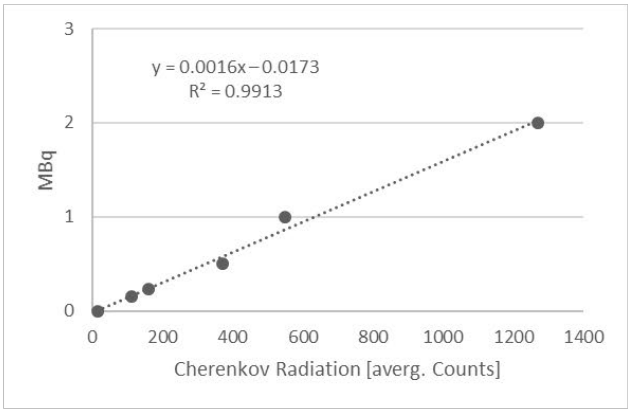
y = 0.0016x − 0.0173
R² = 0.9913
MBq
0
1
2
3
0
200
400
600
800
1000
1200
1400
Cherenkov Radiation [averg. Counts]

C

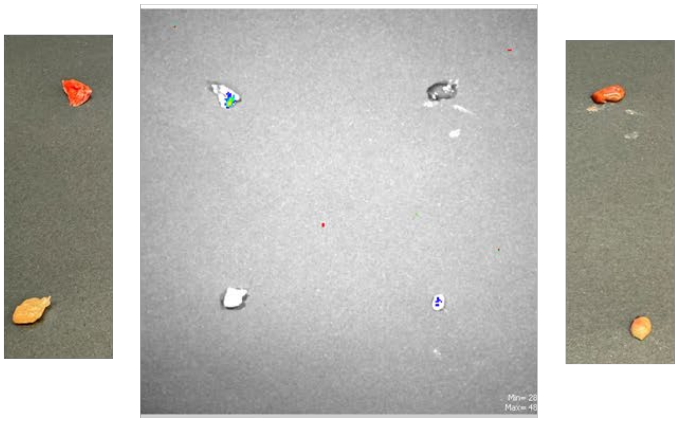

Supplemental Fig. 6: Representative Cherenkov radiation image of fully filled vials including activity description (**A**). Standard calibration curve of average counts plotted against decay corrected MBq of the respective vials filled with [^{18}F]FDG (**B**). Representative ex vivo Cherenkov radiation measurements of lung (top left), liver (top right), muscle (bottom left) and WAT (bottom right) 60 min after injection of 30 MBq [^{18}F]FDG of a KPAr mouse (**C**).

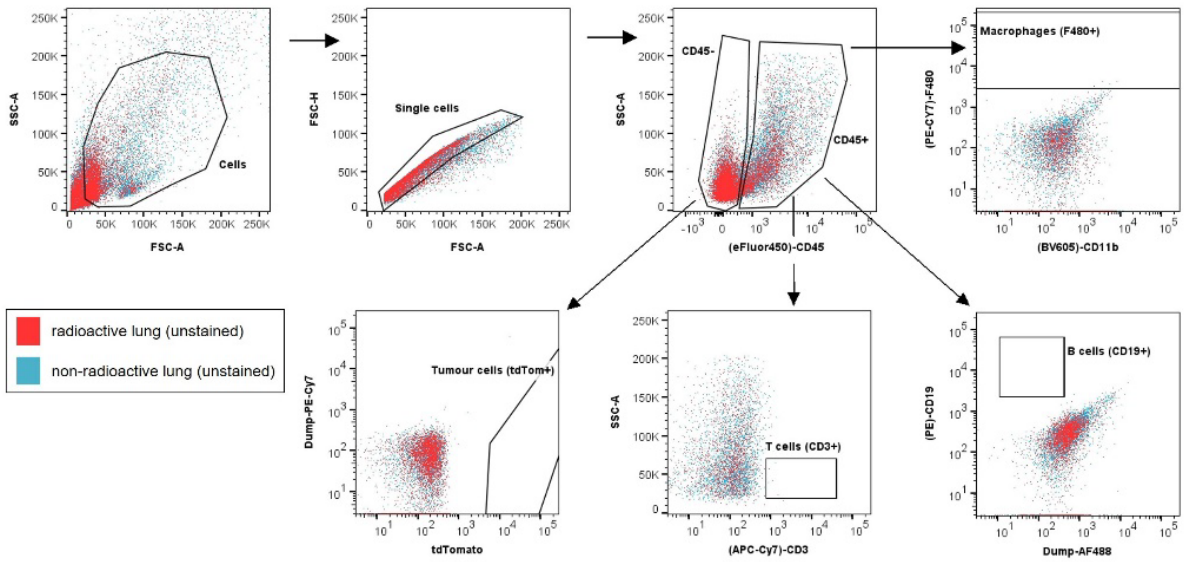

Supplemental Fig. 7: Cell sorting overlay from unstained radioactive lung (WT; red) and non-radioactive lung (WT; blue).

Supplemental Tables:

Supplemental Table 1: Cocktail 3 cell Sorting and radioFlow results.

Cocktail 3	tdTom$^+$ (tumor cells)	CD3$^+$ (T cells)	CD19$^+$ (B cells)	F4/80$^+$ (MΦ)
KPr (n=3)				
% Cell No	23 ±12	16 ±5	46 ±9	16 ±5
% CPM	5 ±3	10 ±6	54 ±3	31 ±5
% CPM/10^5	6 ±1	14 ±2	29 ±2	51 ±2
KPAr (n=4)				
% Cell No	23 ±7	9 ±1	46 ±4	21 ±2
% CPM	8 ±4	4 ±2	53 ±1	35 ±6
% CPM/10^5	9 ±2	14 ±6	32 ±3	46 ±7

Supplemental Table 2: Calculate dose rate for radioFlow analysis.

	kBq		**mSv/h (sum)** 30 cm distance, no shielding		**mSv/a** (once/week for 40 weeks) 30 cm distance, no shielding	
Cell Suspension (before cell sorting)	**Spleen**	**Lung**	**Spleen**	**Lung**	**Spleen**	**Lung**
lowest activity	32	39	4.5E-05	6.00E-05	0.002	0.002
highest activity	89	207	0.00013	0.00031	0.005	0.013
average activity	60	90	9.00E-05	0.000135	0.004	0.005
BED (n=bananas)				1.35	40	50
Dental X-ray (n=times)						1

Dose rates were calculated form spleen and lung from the lowest and highest activities measured; n=8 (kBq for total organ). The kBq were used to calculate the dose rate mSv/h (unshielded) and at a realistic distance of 30 cm from the cell sorting device. For 40 measurements, this calculation resulted in 40-50 banana equivalent doses (BED), which is equivalent to the dose rate of eating 40-50 bananas per year or one dental x-ray.